Journal of Atomic, Molecular, Condensate & Nano Physics
Vol. 6, No. 3, pp. 103–113, 2019
ISSN 2349-2716 (online); 2349-6088 (print)
Published by RGN Publications

http://www.rgnpublications.com

DOI: 10.26713/jamcnp.v6i3.1295

Effect of Dense Plasma Environment on the Spectroscopic Properties of He-like Ca^{18+} Ion

Research Article

Dishu Dawra[1], Mayank Dimri[1,2], A. K. Singh[1,2,*], Alok K. S. Jha[3] and Shougaijm Somorendro Singh[1]

[1] *Department of Physics and Astrophysics, University of Delhi, Delhi 110 007, India*
[2] *Department of Physics, Deen Dayal Upadhyaya College (University of Delhi), Delhi 110 078, India*
[3] *Department of Physics, Kirori Mal College (University of Delhi), Delhi 110 007, India*
***Corresponding author:** avni.physics@gmail.com

Abstract. Plasma shielding effects on the energy levels and radiative properties of He-like Ca^{18+} ion under dense plasma conditions have been studied. For this purpose, the multiconfiguration Dirac-Fock method has been implemented by incorporating the ion sphere model potential as a modified interaction potential between the electron and the nucleus. To check the authenticity of our results, independent calculations have been performed using the modified relativistic configuration interaction method. It is observed that the transition energies associated with $\Delta n = 0$ transitions are blue shifted, whereas red shifted for $\Delta n \neq 0$ transitions. The variation in transition probabilities and weighted oscillator strengths with plasma densities has also been analyzed. The present results should be beneficial in the plasma modeling and fusion plasma research applications.

Keywords. Strongly coupled plasma; Atomic structure; Radiative properties

PACS. 32.70.Cs; 32.70.Jz; 52.27.Gr

Received: September 13, 2019 **Accepted:** October 10, 2019

1. Introduction

During the last few decades, the investigation of structural properties of atomic systems in strongly coupled plasma environment has been an important area of research due to the potential applications in astrophysical systems, laser produced plasmas, X-ray lasers, inertial

confinement fusion, and plasma spectroscopy [1–4]. In such an environment, the interaction between the atomic nucleus and bound electrons is screened by the neighbouring ions and free electrons. This modified interaction gives rise to continuum lowering and affects the atomic structure and transition properties of the ions, when compared with free systems.

The plasma environment can be classified into weakly and strongly coupled plasma according to the value of the plasma coupling strength (Γ), which is defined as the ratio of average electrostatic energy to thermal energy. The case $\Gamma < 1$ denotes a weakly coupled plasma, whereas $\Gamma \geq 1$ signifies a strongly coupled plasma [5,6]. In the strongly coupled plasma, the screening of the nuclear Coulomb interaction by the free electrons is described by the ion sphere model. The ion sphere model assumes that each ion is enclosed in a spherically symmetric cell containing the exact number of electrons to sustain charge neutrality of the system.

Extensive theoretical investigations have been carried out in the past to model the influence of plasma environment on the spectroscopic properties of two-electron system using ion-sphere model. Sil *et al*. [7, 8] have analyzed the effect of strongly coupled plasma on the electronic structure and transition properties of He-like ions within the non-relativistic and relativistic framework. The exchange energy shifts between the $1s^2 \rightarrow 1s2p$ ($^3P_1$,$^1P_1$) lines of Al^{11+} ion immersed in dense plasma environment have been investigated by Li *et al*. [9] using the self-consistent field method. Further, Rodriguez *et al*. [10] have studied the effect of plasma screening in the atomic magnitudes of non-hydrogenic ions using the relativistic detailed configuration accounting approach. Bhattacharya *et al*. [11] have carried out non-relativistic structure calculations of two-electron ions in a strongly coupled plasma environment within the framework of Rayleigh-Ritz variation principle in Hylleraas coordinates. Plasma environment effects on the atomic structure of various ions have been estimated by Belkhiri *et al*. [12] using the *Flexible Atomic Code* (FAC) and *Cowan ATomic Structure* (CATS) code. Furthermore, Li *et al*. [13, 14] have investigated the atomic structure and transition properties of He-like Al^{11+} and Ar^{16+} ions in dense plasma using the modified *general-purpose relativistic atomic structure package* (GRASP2K). Recently, Chen *et al*. [**?**, 15–19] have studied the energies and radiative properties of highly charged ions within dense plasma using both non-relativistic and relativistic methods.

As far as we know, there are no experimental and theoretical results available for He-like Ca^{18+} ion immersed in a strongly coupled plasma, therefore in the present work, we have presented the energy levels and radiative properties of this ion in the isolated condition as well as within the plasma environment using the ion sphere model. The reason for choosing Ca^{18+} ion is due to the fact that the spectroscopic properties of He-like ions have considerable importance in astrophysical and laboratory plasmas [20]. For this purpose, we have implemented the extensively used *multiconfiguration Dirac-Fock* (MCDF) method incorporating the ion sphere model potential as a modified interaction potential between the nucleus and the electron. Finally, to assess the accuracy and reliability of our results, parallel calculations have been performed using the modified relativistic configuration interaction method implemented within the modified *Flexible Atomic Code* (FAC).

This paper is structured as follows: In Section 2, we have briefly outlined the theoretical procedures adopted in our fully relativistic calculations. Section 3 deals with the discussion of our results. The implications of the present work are summarized in Section 4.

2. Theoretical Methods

In this section, we have presented a brief resume of the theoretical approaches adopted to account for the plasma screening effects on the considered system. The ion sphere model assumes that the ion is represented by a point-like nucleus having nuclear charge Z, embedded at the centre of a spherical cavity comprising of sufficient electrons to ensure overall neutrality of the ion sphere.

The fully relativistic MCDF method, revised by Norrington [21] and formerly developed by Grant *et al*. [22] has been employed in our calculations. This method has also been successfully employed in our previous works [23–25]. In order to consider the influence of plasma environment on the spectral properties, the Dirac-Coulomb Hamiltonian containing all the dominant interactions can be written as

$$\widehat{H}^{DC} = \sum_{i=1}^{N} \widehat{H}_i + \sum_{i=1}^{N-1} \sum_{j=i+1}^{N} \frac{1}{|\hat{r}_i - \hat{r}_j|}, \tag{1}$$

where $\widehat{H}_i$ is the one-electron Hamiltonian, and is expressed as

$$\widehat{H}_i = c\boldsymbol{\alpha} \cdot \boldsymbol{p} + (\beta - 1)c^2 + V_{IS}(r, R_0). \tag{2}$$

Here, the first two terms depict the relativistic kinetic energy of a bound electron and the last term $V_{IS}(r, R_0)$ represents the modified potential experienced by the bound electron inside the ion sphere, which is given by

$$V_{IS}(r, R_0) = -\frac{Z}{r} + \frac{Z - N_b}{2R_0}\left[3 - \left(\frac{r}{R_0}\right)^2\right], \tag{3}$$

where $R_0 = [3(Z - N_b)/4\pi n_e]^{1/3}$ is the ion sphere radius, N_b is the number of bound electrons which means that $(Z - N_b)$ are the additional and uniformly distributed free plasma electrons inside the ion sphere and n_e is the plasma electron density.

An *atomic state function* (ASF) is expanded in terms of the linear combination of n electronic *configuration state functions* (CSFs)

$$|\psi_\alpha(PJM)\rangle = \sum_{i=1}^{n} C_i(\alpha)|\gamma_i(PJM)\rangle. \tag{4}$$

In the above equation, the CSFs $\gamma_i(PJM)$ are characterized by total angular momentum J, magnetic quantum number M and parity P, respectively. The expansion mixing coefficients $C_i(\alpha)$ for each CSF satisfy the relation

$$(C_i(\alpha))^\dagger C_j(\alpha) = \delta_{ij}, \tag{5}$$

allowing ASFs to satisfy the condition of orthonormality, α stands for the orbital occupation numbers, coupling, etc. The CSFs are the sum of products of four-component spin-orbitals having the form

$$\phi_{nkm} = \frac{1}{r}\begin{pmatrix} P_{nk}(r) & \chi_{km}(\theta, \phi, \sigma) \\ -iQ_{nk}(r) & \chi_{-km}(\theta, \phi, \sigma) \end{pmatrix}, \tag{6}$$

where n denotes the principal quantum number, k is the Dirac angular quantum number, $P_{nk}(r)$ and $Q_{nk}(r)$ are large and small components of one-electron radial functions and

$\chi_{km}(\theta,\phi)$ is the the spinor spherical harmonic function. Regarding the electrically neutral conditions assumed by the ion sphere model, the radial components of the wavefunction satisfy the normalization condition given by

$$\int_0^\infty [{P_{nk}}^2(r) + Q_{nk}^2(r)]dr = 1. \tag{7}$$

For higher values of free electron density, the bound electron wavefunctions may not be equal to 0 outside the ion sphere.

To elucidate the accuracy of our MCDF results, analogous calculations have been carried out using the *Flexible Atomic Code* (FAC). FAC employs a fully relativistic approach in which the basis wavefunctions are derived from the local central potential [26]. For the N-electron atom or ion immersed in dense plasma, the relativistic Hamiltonian can be written as

$$\widehat{H} = \sum_{i=1}^{N} \widehat{H}_D(i) + \sum_{i<j}^{N} \frac{1}{r_{ij}}, \tag{8}$$

where the single-electron Dirac-Hamiltonian $\widehat{H}_D(i)$ is defined as

$$\widehat{H}_D(i) = c\boldsymbol{\alpha}\cdot\boldsymbol{p} + (\boldsymbol{\beta}-1)c^2 + V_{IS}(r,R_0). \tag{9}$$

The approximate ASFs are given by mixing the basis states, ϕ_v, with same symmetries

$$\Psi = \sum_v b_v \phi_v, \tag{10}$$

where diagonalization of the total Hamiltonian yields the mixing coefficients b_v.

3. Results and Discussion

In the present work, the fully relativistic MCDF method has been modified by incorporating the ion sphere model potential to study the effect of dense plasma background. For the calculation of the wavefunctions and energy levels, we have considered the configurations, namely, $1s^2$, $1s2s$, $1s2p$, $1s3s$, $1s3p$, $1s3d$, $1s4s$, $1s4p$, $1s4d$, $2s^2$, $2s2p$, $2p^2$, $2s3s$, $2s3p$, $2s3d$, $2s4s$, $2s4p$ and $2s4d$ which give rise to a total of 57 fine structure energy levels. The *configuration interaction* (CI) has been taken into account among the aforementioned 18 configurations and the option of *extended average level* (EAL) has been used to optimize the trace of the Hamiltonian. The contributions from the *Breit interaction* (BI) and *quantum electrodynamics* (QED) corrections are fully taken into consideration.

Table 1 presents the binding energies at different electron densities ranging from 1.0×10^{22} to 1.0×10^{24} cm^{-3} for Ca^{18+} ion using MCDF and FAC methods. It can be seen that results from both the theoretical methods are in good agreement with each other within 0.02%. The variation of electron binding energy with respect to free electron density is plotted in Figure 1. It is evident from the figure that the binding energy is decreasing monotonically with increase in electron density. This trend is an outcome of the increase in the number of free electrons inside the ion sphere with increasing electron densities, thus strengthening the effect of screening on the nucleus by the free electrons.

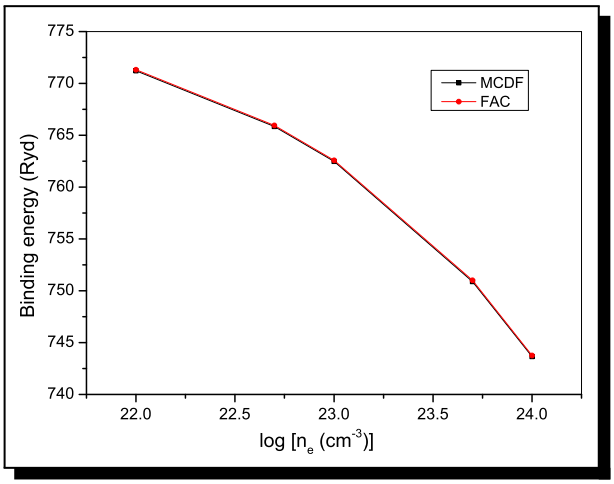

Figure 1. Variation of binding energy for Ca^{18+} ion with the free electron density

Table 1. Variation of binding energy (in Ryd) at different electron densities (n_e in cm^{-3}) for Ca^{18+} ion

n_e	Binding energy		Relative difference (%)
	MCDF	FAC	MCDF vs FAC
0	778.7846	778.8947	0.0141
1.0×10^{22}	771.2137	771.3239	0.0143
5.0×10^{22}	765.8388	765.9490	0.0144
1.0×10^{23}	762.4743	762.5845	0.0145
5.0×10^{23}	750.8972	751.0078	0.0147
1.0×10^{24}	743.6519	743.7623	0.0148

The energy levels (with respect to the ground state) belonging to the configurations $1snl$ ($n = 2,3$) of He-like Ca^{18+} ion at different electron densities are given in Table 2 using the MCDF and FAC methods. As one can observe, our MCDF results agree well with the FAC ones which affirms the accuracy and reliability of our results. For comparison purposes, the results for the unscreened case are also tabulated along with the *National Institute of Standards and Technology* (NIST) [27] recommended values. One can see that there is good agreement between the present theoretical results and the observed values from the NIST database. It can be noticed that when dense plasma effects are taken into account, the excitation energies decrease rapidly with increase in free electron density. Further, our presented results indicate that the effect of plasma screening on the excitation energies is very small at a lower electron density, whereas it is more pronounced at a higher electron density. For example, the effect of dense plasma on the excitation energies calculated using MCDF method is about 0.01 and 0.47 eV, while about 0.62 and 4.52 eV for $1snp\ ^3P_1^o$ ($n = 2,3$) levels at the electron densities $n_e = 1.0 \times 10^{22}$ and 1.0×10^{24} cm^{-3}, respectively.

Table 2. Transition energies (in Ryd) at different electron densities (n_e in cm^{-3}) for the He-like Ca^{18+} ion in plasmas

Level	NIST [27]	Free ion	1.0×10^{22}	5.0×10^{22}	1.0×10^{23}	5.0×10^{23}	1.0×10^{24}
1s2s $^3S_1$	283.7882	283.6124[a]	283.6118[a]	283.6092[a]	283.6061[a]	283.5809[a]	283.5494[a]
		283.6979[b]	283.6973[b]	283.6948[b]	283.6917[b]	283.6667[b]	283.6393[b]
1s2p $^3P^o_0$	285.3436	285.1593[a]	285.1589[a]	285.1571[a]	285.1548[a]	285.1367[a]	285.1140[a]
		285.2376[b]	285.2371[b]	285.2353[b]	285.2331[b]	285.2154[b]	285.1955[b]
1s2p $^3P^o_1$	285.4185	285.2289[a]	285.2284[a]	285.2266[a]	285.2243[a]	285.2062[a]	285.1834[a]
		285.3084[b]	285.3079[b]	285.3062[b]	285.3039[b]	285.2861[b]	285.2664[b]
1s2s $^1S_0$	285.4858	285.4339[a]	285.4333[a]	285.4308[a]	285.4276[a]	285.4024[a]	285.3709[a]
		285.3754[b]	285.3747[b]	285.3722[b]	285.3689[b]	285.3430[b]	285.3133[b]
1s2p $^3P^o_2$	285.7404	285.5524[a]	285.5519[a]	285.5501[a]	285.5478[a]	285.5294[a]	285.5064[a]
		285.6338[b]	285.6333[b]	285.6315[b]	285.6293[b]	285.6113[b]	285.5913[b]
1s2p $^1P^o_1$	286.8105	286.6848[a]	286.6843[a]	286.6825[a]	286.6801[a]	286.6616[a]	286.6384[a]
		286.7295[b]	286.7290[b]	286.7272[b]	286.7249[b]	286.7064[b]	286.6869[b]
1s3s $^3S_1$	335.9927	335.7865[a]	335.7831[a]	335.7696[a]	335.7527[a]	335.6174[a]	335.4469[a]
		335.8717[b]	335.8683[b]	335.8549[b]	335.8380[b]	335.7031[b]	335.5337[b]
1s3p $^3P^o_0$	336.4222	336.2198[a]	336.2168[a]	336.2048[a]	336.1899[a]	336.0702[a]	335.9254[a]
		336.3044[b]	336.3014[b]	336.2895[b]	336.2746[b]	336.1552[b]	336.0049[b]
1s3s $^1S_0$	336.4392	336.2405[a]	336.2685[a]	336.2547[a]	336.2107[a]	336.0993[a]	335.9194[a]
		336.3326[b]	336.3292[b]	336.3155[b]	336.2983[b]	336.1603[b]	335.9873[b]
1s3p $^3P^o_1$	336.4422	336.2719[a]	336.2376[a]	336.2256[a]	336.2375[a]	336.0908[a]	335.9398[a]
		336.3257[b]	336.3227[b]	336.3108[b]	336.2959[b]	336.1764[b]	336.0260[b]
1s3p $^3P^o_2$	336.5387	336.3367[a]	336.3337[a]	336.3217[a]	336.3067[a]	336.1862[a]	336.0344[a]
		336.4225[b]	336.4195[b]	336.4076[b]	336.3926[b]	336.2725[b]	336.1213[b]
1s3d $^3D_1$		336.5709[a]	336.5688[a]	336.5603[a]	336.5497[a]	336.4649[a]	336.3581[a]
		336.6625[b]	336.6604[b]	336.6519[b]	336.6414[b]	336.5570[b]	336.4501[b]
1s3d $^3D_2$		336.5701[a]	336.5680[a]	336.5595[a]	336.5489[a]	336.4641[a]	336.3573[a]
		336.6617[b]	336.6596[b]	336.6511[b]	336.6406[b]	336.5562[b]	336.4493[b]
1s3d $^3D_3$		336.6085[a]	336.6064[a]	336.5979[a]	336.5873[a]	336.5022[a]	336.3951[a]
		336.7002[b]	336.6981[b]	336.6897[b]	336.6791[b]	336.5944[b]	336.4873[b]
1s3d $^1D_2$		336.6222[a]	336.6201[a]	336.6116[a]	336.6010[a]	336.5158[a]	336.4086[a]
		336.7135[b]	336.7114[b]	336.7030[b]	336.6924[b]	336.6076[b]	336.5004[b]
1s3p $^1P^o_1$	336.8306	336.6507[a]	336.6477[a]	336.6355[a]	336.6203[a]	336.4980[a]	336.3441[a]
		336.7213[b]	336.7183[b]	336.7061[b]	336.6909[b]	336.5689[b]	336.4152[b]

[a] Present MCDF. [b] Present FAC.

Figures 2 and 3 display the variation of transition energies of the 1s2s $^3S_1 \rightarrow 1s2p\ ^3P^o_0$ and 1s3s $^3S_1 \rightarrow 1s3d\ ^3D_2$ transitions of He-like Ca^{18+} ion for different electron densities using MCDF method. As can be seen, the transition energies associated with the $\Delta n = 0$ transitions are blue shifted i.e. increasing rapidly with increasing free electron densities. Moreover, the variation of the transition energies of the $1s^2\ ^1S_0 \rightarrow 1snp\ ^1P^o_1$ ($n = 2, 3$) transitions as a function of electron density is shown in Figures 4 and 5. It can be inferred that the transition energies

associated with the $\Delta n \neq 0$ transitions are red shifted i.e. decreasing rapidly with increase in free electron density.

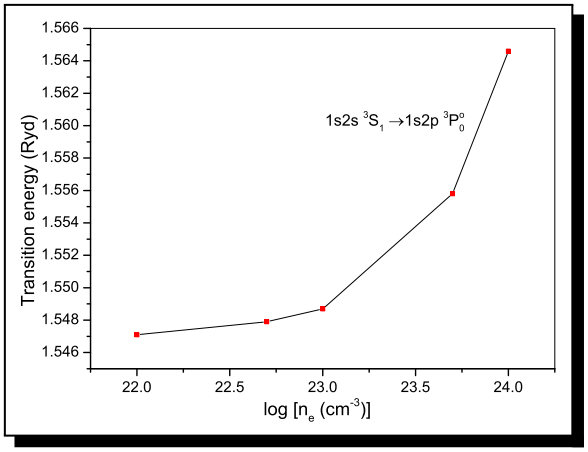

Figure 2. Variation of transition energy of the $1s2s\ ^3S_1 \rightarrow 1s2p\ ^3P^o_0$ transition with the free electron density

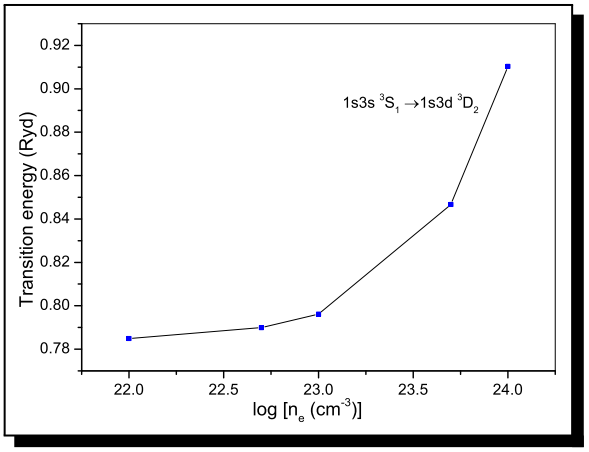

Figure 3. Variation of transition energy of the $1s3s\ ^3S_1 \rightarrow 1s3d\ ^3D_2$ transition with the free electron density

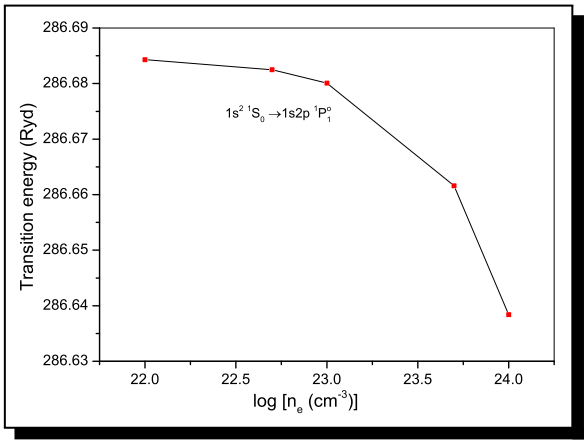

Figure 4. Variation of transition energy of the $1s^2\ ^1S_0 \rightarrow 1s2p\ ^1P^o_1$ transition with the free electron density

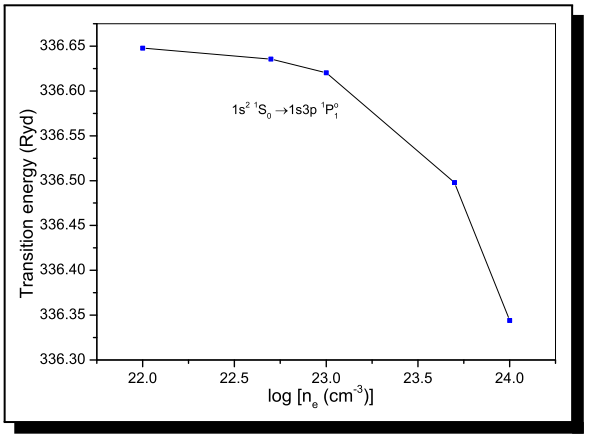

Figure 5. Variation of transition energy of the $1s^2\ ^1S_0 \rightarrow 1s3p\ ^1P^o_1$ transition with the free electron density

The transition probabilities (A) and weighted oscillator strengths (gf) of the intercombination $1s^2\ ^1S_0 \rightarrow 1snp\ ^3P^o_1$ $(n = 2,3)$ and resonance $1s^2\ ^1S_0 \rightarrow 1snp\ ^1P^o_1$ $(n = 2,3)$ transitions of He-like Ca^{18+} ion are provided in Tables 3 and 4 using MCDF method. Emphasis has been placed on the above mentioned transitions as they are especially useful for plasma diagnostics. In Figure 6, we show the variation of transition probabilities of these transitions with respect to free electron densities. Inspection of this Figure shows that the transition probabilities for all these transitions decrease with increasing plasma densities. Moreover, a similar trend has been observed for the weighted oscillator strengths.

Table 3. Transition probabilities (A in s^{-1}) and weighted oscillator strengths (gf) at different electron densities (n_e in cm^{-3}) for the intercombination $1s^2\ ^1S_0 \rightarrow 1snp\ ^3P^o_1$ ($n = 2,3$) transitions of Ca^{18+} ion

n_e	$1s^2\ ^1S_0 \rightarrow 1s2p\ ^3P^o_1$		$1s^2\ ^1S_0 \rightarrow 1s3p\ ^3P^o_1$	
	A ($\times 10^{12}$)	gf ($\times 10^{-2}$)	A ($\times 10^{12}$)	gf ($\times 10^{-3}$)
0	4.5814	2.1032	1.4421	4.7640
1.0×10^{22}	4.5813	2.1032	1.4419	4.7633
5.0×10^{22}	4.5810	2.1031	1.4410	4.7607
1.0×10^{23}	4.5806	2.1029	1.4399	4.7575
5.0×10^{23}	4.5775	2.1017	1.4309	4.7311
1.0×10^{24}	4.5735	2.1002	1.4196	4.6979

Table 4. Transition probabilities (A in s^{-1}) and weighted oscillator strengths (gf) at different electron densities (n_e in cm^{-3}) for the resonance $1s^2\ ^1S_0 \rightarrow 1snp\ ^1P^o_1$ ($n = 2,3$) transitions of Ca^{18+} ion

n_e	$1s^2\ ^1S_0 \rightarrow 1s2p\ ^1P^o_1$		$1s^2\ ^1S_0 \rightarrow 1s3p\ ^1P^o_1$	
	A ($\times 10^{14}$)	gf ($\times 10^{-1}$)	A ($\times 10^{13}$)	gf ($\times 10^{-1}$)
0	1.7132	7.7852	4.9876	1.6436
1.0×10^{22}	1.7132	7.7852	4.9870	1.6435
5.0×10^{22}	1.7132	7.7852	4.9847	1.6428
1.0×10^{23}	1.7131	7.7852	4.9817	1.6420
5.0×10^{23}	1.7129	7.7852	4.9581	1.6354
1.0×10^{24}	1.7127	7.7857	4.9293	1.6274

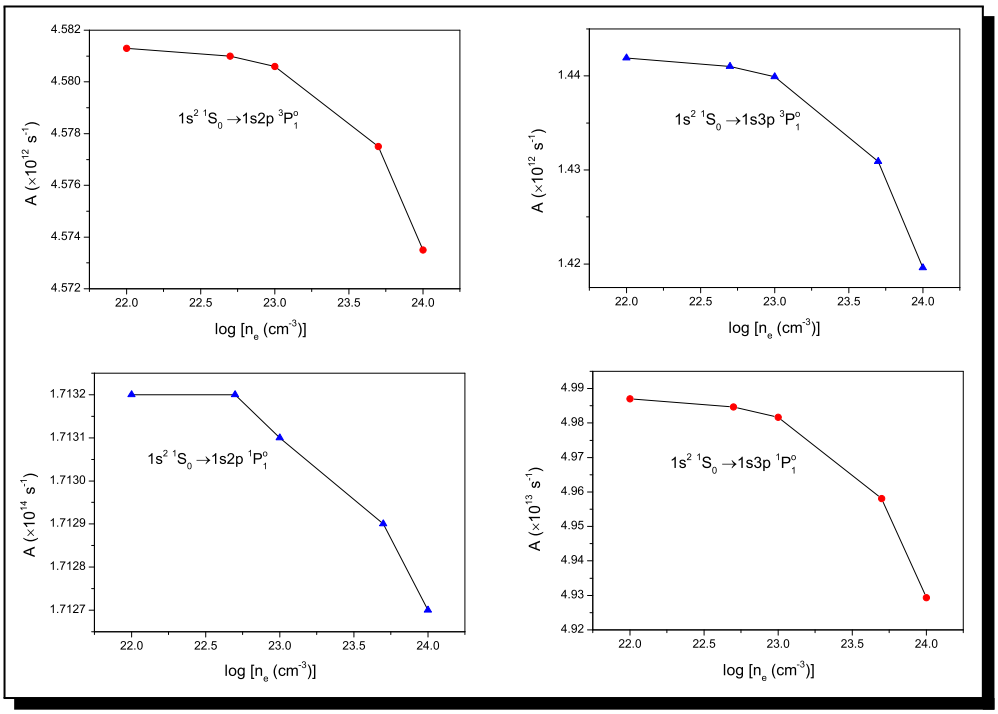

Figure 6. Variation of the transition probabilities (A) for the intercombination $1s^2\ ^1S_0 \rightarrow 1snp\ ^3P^o_1$ ($n = 2,3$) and the resonance $1s^2\ ^1S_0 \rightarrow 1snp\ ^1P^o_1$ ($n = 2,3$) transitions with the free electron density

To assess the accuracy of radiative parameters, the gf Babushkin/Coulomb gauge ratios of the above transitions are plotted in Figure 7. As shown, the ratios are very close to unity which implies that our MCDF results are in better agreement in the two different gauges. Our presented results can satisfy the demand for precision in consideration of influence of plasma screening on the atomic structure and radiative properties of the concerned ion.

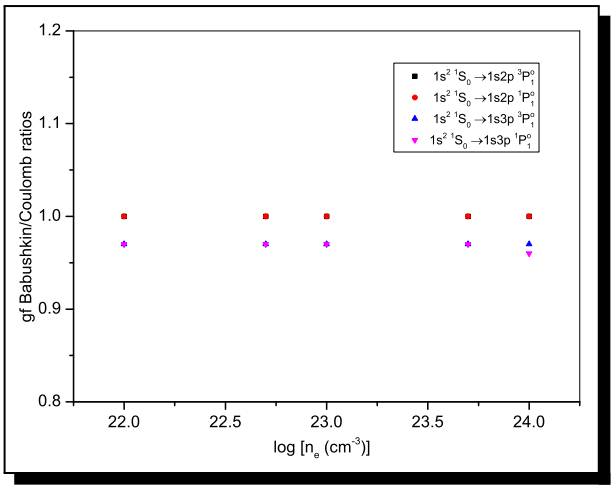

Figure 7. The Babushkin/Coulomb ratios of oscillator strengths for He-like Ca^{18+} ion in dense plasma

4. Conclusion

In the present study, the MCDF method has been implemented by incorporating the ion sphere model potential to study the effect of dense plasma environment on the energy levels and radiative properties of He-like Ca^{18+} ion. For comparison purposes, independent calculations have been performed using modified FAC. We found a good agreement between our MCDF and FAC results which affirms the accuracy and reliability of our results. Also, our unscreened results for this ion match well with the observed values of NIST. Our present calculations show that the influence of plasma screening reduces the excitation energies over the whole electron density range considered. Moreover, the transition energies associated with $\Delta n = 0$ transitions are blue shifted whereas red shifted for $\Delta n \neq 0$ transitions. It is observed that the presence of dense plasma environment has a significant effect on the transition probabilities and weighted oscillator strengths of He-like Ca^{18+} ion embedded in plasma. To the best of our knowledge, the present study is the first effort to analyze the influence of plasma screening on the considered ion. We believe that the present results should be advantageous in the plasma modeling and fusion plasma research applications.

Acknowledgements

This work was carried out at Deen Dayal Upadhyaya College, University of Delhi, India. The authors gratefully acknowledge the financial assistance provided by SERB, the Department of Science and Technology, Govt. of India under the research grant No. EMR/2016/001203.

Competing Interests

The authors declare that they have no competing interests.

Authors' Contributions

All the authors contributed significantly in writing this article. The authors read and approved the final manuscript.

References

[1] M. S. Murillo, J. Weisheit, S. B. Hansen and M. Dharma Wardana, *Phys. Rev. E* **87**, 063113 (2013), DOI: 10.1103/PhysRevE.87.063113.

[2] B. Saha and S. Fritzsche, *J. Phys. B: At. Mol. Opt. Phys.* **40**, 259 (2007), DOI: 10.1088/0953-4075/40/2/002.

[3] M. Nantel, G. Ma, S. Gu, C. Y. Cote, J. Itatani and D. Umstadter, *Phys. Rev. Lett.* **80**, 4442 (1998), DOI: 10.1103/PhysRevLett.80.4442.

[4] S. Skupsky, *Phys. Rev. A* **21**, 1316 (1980), DOI: 10.1103/PhysRevA.21.1316.

[5] S. Ichimaru, *Rev. Mod. Phys.* **54**, 1017 (1982), DOI: 10.1103/RevModPhys.54.1017.

[6] M. S. Murillo and J. C. Weisheit, *Phys. Rep.* **302**, 1 (1998), DOI: 10.1016/S0370-1573(98)00017-9.

[7] A. Sil and P. Mukherjee, *Int. J. Quantum Chem.* **106**, 465 (2006), DOI: 10.1002/qua.20733.

[8] A. Sil, J. Anton, S. Fritzsche, P. Mukherjee and B. Fricke, *Eur. Phys. J. D* **55**, 645 (2009), DOI: 10.1140/epjd/e2009-00258-6.

[9] X. Li, Z. Xu and F. Rosmej, *J. Phys. B: At. Mol. Opt. Phys.* **39**, 3373 (2006), DOI: 10.1088/0953-4075/39/16/019.

[10] R. Rodriguez, J. M. Gil and R. Florido, *Phys. Scr.* **76**, 418 (2007), DOI: 10.1088/0031-8949/76/5/002.

[11] S. Bhattacharyya, J. Saha and T. Mukherjee, *Phys. Rev. A* **91**, 042515 (2015), DOI: 10.1103/PhysRevA.91.042515.

[12] M. Belkhiri, C. J. Fontes and M. Poirier, *Phys. Rev. A* **92**, 032501 (2015), DOI: 10.1103/PhysRevA.92.032501.

[13] X.-F. Li, G. Jiang, H.-B. Wang, M. Wu and Q. Sun, *Phys. Scr.* **92**, 075401 (2017), DOI: 10.1088/1402-4896/aa7000.

[14] X.-F. Li and G. Jiang, *Chin. Phys. B* **27**, 073101 (2018), DOI: 10.1088/1674-1056/27/7/073101.

[15] Z. B. Chen, K. Ma, Y. L. Ma and K. Wang, *Phys. Plasmas* **26**, 082101 (2019), DOI: 10.1063/1.5100850.

[16] Z.-B. Chen, *J. Quant. Spectrosc. Radiat. Transf.* **237**, 106615 (2019).

[17] Z.-B. Chen, *J. Electron Spectros. Relat. Phenomena* **237**, 146894 (2019), DOI: 10.1016/j.elspec.2019.146894.

[18] Z.-B. Chen, K. Wang, K. Ma and F. Hu, *J. Quant. Spectrosc. Radiat. Transf.* **236**, 106584 (2019), DOI: 10.1016/j.jqsrt.2019.106584.

[19] Z.-B. Chen, *Radiat. Phys. Chem.* **166**, 108508 (2020), DOI: 10.1016/j.radphyschem.2019.108508.

[20] K. M. Aggarwal and F. P. Keenan, *Phys. Scr.* **85**, 025306 (2012), DOI: 10.1088/0031-8949/85/02/025306.

[21] P. H. Norrington, http://amdpp.phys.strath.ac.uk/UKAPAP/codes.html.

[22] I. Grant, J. McKenzie, P. Norrington, M. Mayers and N. Pyper, Comput. Phys. Commun. 21, 207 (1980), DOI: 10.1016/0010-4655(80)90041-7.

[23] A. Singh, D. Dawra, M. Dimri, A. K. Jha and M. Mohan, *Phys. Plasmas* **26**, 062704 (2019), DOI: 10.1063/1.5100565.

[24] A. Singh, M. Dimri, D. Dawra, A. K. Jha, N. Verma and M. Mohan, *Radiat. Phys. Chem.* **156**, 174 (2019), DOI: 10.1016/j.radphyschem.2018.11.002.

[25] A. Singh, M. Dimri, D. Dawra, A. K. Jha and M. Mohan, *Can. J. Phys.* **97**, 436 (2019), DOI: 10.1139/cjp-2018-0218.

[26] M. F. Gu, *Can. J. Phys.* **86**, 675 (2008), DOI: 10.1139/p07-197.

[27] A. Kramida, Yu. Ralchenko, J. Reader and NIST ASD Team, NIST Atomic Spectra Database (ver. 5.6.1), [Online], available: https://physics.nist.gov/asd [2019, June 20]. National Institute of Standards and Technology, Gaithersburg, MD. (2018).